ACADÉMIE
DES SCIENCES
INSTITUT DE FRANCE

Comptes Rendus
Physique

Frank Stefani , Sten Anders, Sven Eckert, Nico Freyer, Gunter Gerbeth, André Giesecke, Thomas Gundrum, Peter Kaever, Vivaswat Kumar, Federico Pizzi, Dirk Räbiger, Ján Šimkanin, Christian Steglich, Tobias Vogt, Nicole Wagner and Gerald Wedel

The DRESDYN precession experiment

Volume 25, Special Issue S3 (2024), p. 629-647

Online since: 16 December 2024

Part of Special Issue: Geophysical and astrophysical fluid dynamics in the laboratory
Guest editors: Stephan Fauve (Laboratoire de Physique de l'ENS, CNRS, PSL Research University, Sorbonne Université, Université Paris Cité, Paris, France) and Michael Le Bars (CNRS, Aix Marseille Univ, Centrale Marseille, IRPHE, Marseille, France)

https://doi.org/10.5802/crphys.214

The Comptes Rendus. Physique *are a member of the Mersenne Center for open scientific publishing*
www.centre-mersenne.org — e-ISSN : 1878-1535

ACADÉMIE DES SCIENCES
INSTITUT DE FRANCE

Comptes Rendus. Physique
2024, Vol. 25, Special issue S3, p. 629-647
https://doi.org/10.5802/crphys.214

Research article / *Article de recherche*

Geophysical and astrophysical fluid dynamics in the laboratory / *Dynamique des fluides géophysiques et astrophysiques au laboratoire*

The DRESDYN precession experiment

L'expérience de précession DRESDYN

Frank Stefani [a,*], Sten Anders [a], Sven Eckert [a], Nico Freyer [a], Gunter Gerbeth [a], André Giesecke [a], Thomas Gundrum [a], Peter Kaever [a], Vivaswat Kumar [a], Federico Pizzi [b], Dirk Räbiger [a], Ján Šimkanin [c], Christian Steglich [a], Tobias Vogt [a], Nicole Wagner [a] and Gerald Wedel [a]

[a] Helmholtz-Zentrum Dresden-Rossendorf, Bautzner Landstr. 400, D-01328 Dresden, Germany

[b] Department of Fluid Mechanics, Universitat Politècnica de Catalunya-Barcelona Tech, Barcelona 08034, Spain

[c] Institute of Geophysics of the Czech Academy of Sciences, Boční II/1401, Praha 4-Spořilov 141 31, Czech Republic

E-mails: F.Stefani@hzdr.de (F. Stefani), S.Anders@hzdr.de (S. Anders), S.Eckert@hzdr.de (S. Eckert), N.Freyer@hzdr.de (N. Freyer), G.Gerbeth@hzdr.de (G. Gerbeth), A.Giesecke@hzdr.de (A. Giesecke), Th.Gundrum@hzdr.de (Th. Gundrum), P.Kaever@hzdr.de (P. Kaever), V.Kumar@hzdr.de (V. Kumar), federico.pizzi@upc.edu (F. Pizzi), D.Raebiger@hzdr.de (D. Räbiger), jano@ig.cas.cz (J. Šimkanin), csteglich@gmx.de (C. Steglich), T.Vogt@hzdr.de (T. Vogt), N.Wagner@hzdr.de (N. Wagner), G.Wedel@hzdr.de (G. Wedel)

Abstract. The most ambitious project within the DREsden Sodium facility for DYNamo and thermohydraulic studies (DRESDYN) at Helmholtz-Zentrum Dresden-Rossendorf (HZDR) is the set-up of a precession-driven dynamo experiment. After discussing the scientific background and some results of water pre-experiments and numerical predictions, we focus on the numerous structural and design problems of the machine. We also outline the progress of the construction work and give an outlook for the upcoming experimental campaigns.

Résumé. Le projet le plus ambitieux au sein de l'installation DREsden Sodium pour les études DYNamo et thermohydrauliques (DRESDYN) au Helmholtz-Zentrum Dresden-Rossendorf (HZDR) est la mise en place d'une expérience de dynamo entrainée par précession. Après avoir discuté du contexte scientifique, de quelques résultats d'expériences préliminaires en eau et de prédictions numériques, nous nous concentrons sur les nombreux problèmes structurels et de conception de la machine. Nous décrivons également l'avancement des travaux et donnons un aperçu des campagnes expérimentales prévues.

Keywords. precession, dynamo, sodium.

Mots-clés. précession, dynamo, sodium.

* Corresponding author

Funding. European Research Council (ERC) under the European Union's Horizon 2020 research and innovation program (Grant Agreement No. 787544), Deutsche Forschungsgemeinschaft (Grant No. GI 1405/1-1).

Manuscript received 1 March 2024, revised 29 July 2024, accepted 3 October 2024.

1. Introduction

Hydromagnetic dynamo action in moving electrically conducting fluids is at the root of planetary, stellar and galactic magnetic fields [1]. While dynamo *theory* is now a well-established cornerstone of magnetohydrodynamics [2,3], dynamo *experiments* have been rare due to the enormous technical effort that is required for their successful realization. Yet, the last decades have seen significant progress in this field [4–8], starting with the nearly concurrent successes of the single-scale, Ponomarenko-type dynamo in Riga [9–14] and the two-scale α^2-type dynamo in Karlsruhe [15–18], followed by the von-Kármán-sodium (VKS) experiment in Cadarache [19–23]. Despite, or better, because of the use of impellers with high magnetic permeability [24–26], the latter experiment has shown a wealth of most interesting dynamical effects, including field reversals and excursions, depending on the rotation rates of two impellers. With regard to comparable events the geomagnetic field is known to undergo, these results have spurred new theoretical efforts to understand the underlying physical mechanism(s) in a more generic sense [27–29].

It is here where astronomical, or harmonic, forcings of dynamos come into play [30]. As discussed by Consolini and De Michelis [31] (and later corroborated in a simple α^2-dynamo model [32]) the probability density of the intervals between reversals appears to be governed by a stochastic resonance with the 95-kyr periodicity of the ellipticity of the Earth's orbit. Further paleomagnetic data suggest complementary influences of the other two Milankovic cycles, viz., precession and nutation, on the geodynamo [33]. Tidal forces have also been invoked as possible sources of the (early) geodynamo, although a quantification of the effects of all these forces, and their interaction with more conventional convective dynamo drivers, is still under scrutiny [34]. The same applies to precession as a source of the ancient lunar dynamo [35,36], or of the magnetic field of the asteroid Vesta [37].

Going beyond planets, moons and asteroids, there is growing empirical evidence that the solar dynamo might also be influenced by astronomical forcings. First and foremost, it is the suspicious (though not undisputed, see [38,39]) synchronicity of the Schwabe cycle with the 11.07-yr periodicity of the envelope of the Venus-Earth-Jupiter alignments that points to a possible influence of tides on the dynamo [40–48]. The two-planet spring tides of those planets were recently shown [49,50] to be capable of exciting magneto-Rossby waves with typical periods between 100 and 300 days, whose joint quadratic action indeed comprises a 11.07-yr periodicity that may well be capable of entraining the solar dynamo by parametric resonance. Moreover, longer type-periodicities, such as the Suess–de Vries cycle, could arise as a 193-yr beat period of the primarily synchronized 22.14-yr Hale cycle with the 19.86-yr period of the rosette-shaped motion of the Sun around the barycenter of the solar system. First attempts to apply the underlying orbit-spin coupling [51] to the case of the Sun [52] point to an interesting parallelity with precession (for the specific influence of eccentric orbits on rotating ellipsoids, cp. [53]).

That said, this paper will exclusively concentrate on how to generate, in the lab, a precession driven flow that is prone to dynamo action. Our restriction to precession follows from two general considerations on how to progress from the pioneering experiments in Riga, Karlsruhe and Cadarache towards a more "natural", i.e. truly homogeneous, dynamo. First, we note that any realization of a convection driven dynamo in the lab would be extremely expensive, requiring an enormous heating power and/or vessel size (although this hurdle could possibly

be overcome by using centrifugal buoyancy [54]). Second, among the various candidates of astronomical forcings, precession represents a key paradigm with a relatively straightforward (although challenging) technical implementability. In this regard, the DRESDYN precession experiment may, hopefully, pave the way for later implementations of libration, nutation, tides or changes of the orbital ellipticity.

To get a glimpse on the advantages and limitations of dynamo experiments we compare, in Figure 1, some dimensionless numbers reachable at the DRESDYN machine with those that are accessible by present-day numerics, and those of the geodynamo. This is illustrated in two panels covering (a) the magnetic Reynolds number and the magnetic Prandtl number and (b) the Reynolds number and the Poincaré number. While, evidently, the experiment can go much farther than simulations, it is still way off the reality of the geodynamo.

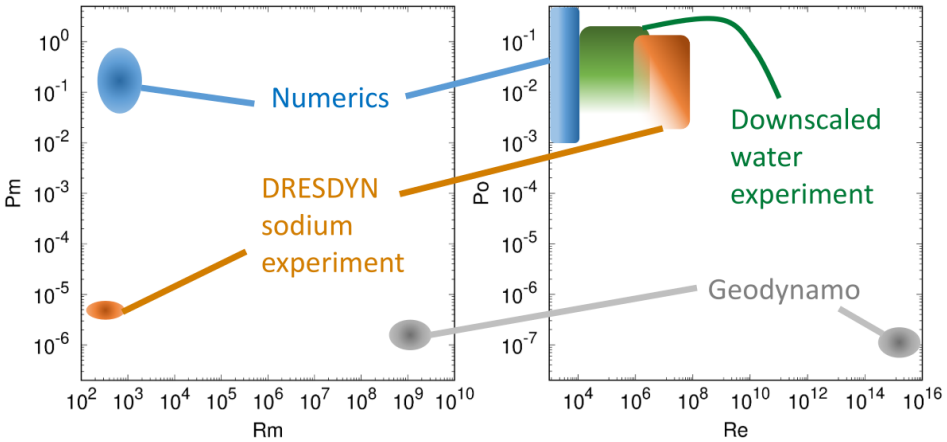

Figure 1. Comparison of various dimensionless numbers of the DRESDYN precession experiment, the 1 : 6 downscaled water experiment, the utilized numerics, and the geodynamo. Using the radius R, the angular frequencies of the rotation and precession, Ω_c and Ω_p, the viscosity ν and the electrical conductivity σ, (a) shows the magnetic Reynolds number $Rm = \mu_0 \sigma R^2 \Omega_c$ and the magnetic Prandtl number $Pm = \nu \mu_0 \sigma$, while (b) shows the (hydrodynamic) Reynolds number $Re = R^2 \Omega_c / \nu$ and the Poincaré number $Po = \Omega_p / \Omega_c$.

In the next section, we delineate the fundamental hydrodynamics behind precession-driven flows in cylindrical geometry, and discuss the dependence of the flow on the main parameters such as Reynolds number, precession ratio, and nutation angle. Then we explore the suitability of the emerging flows for dynamo action and indicate some optimum experimental parameters.

Section 3 is then devoted to the more technical aspects of the experiment, including the massive basement, the main parts of the platform and the design of the rotation vessel.

The paper will close with a summary and an outlook on the upcoming experimental campaigns.

2. Precession driven flows in cylindrical geometry, and their dynamo action

Precession-driven flows were first investigated for the case of an inviscid fluid in a spheroidal cavity [55,56] for which an analytical solution was obtained assuming uniform vorticity. This so-called Poincaré solution was later extended by Busse [57] to the weakly nonlinear regime, including the viscous effects in boundary layers. Meanwhile, the theory of precession-driven flows has

been extended to other geometries, and a couple of corresponding experiments were dedicated to understand particular features such as instabilities [58–60], large-scale vortex formation [61], the transition to turbulence and its hysteretic behaviour [62–67]. Dynamo action for precession-driven flows was numerically found in various geometries [68–75]. Most remarkably, a field amplification by a factor of three was reached in an early liquid-sodium experiment by Gans [76].

In this section, we will first present the mathematical and numerical basics of precession driven flows in cylindrical geometry and some details of a corresponding down-scaled water experiment. Then we will compare the obtained numerical and experimental results for different precession ratios and nutation angles. Based on those findings we will discuss some predictions for dynamo action in the large machine.

2.1. *Basic theory*

Assuming an incompressible fluid with constant density ρ, the Navier–Stokes equation in the doubly-rotating frame (henceforth called the *container frame*),

$$\frac{\partial \boldsymbol{u}}{\partial t} + \boldsymbol{u}\cdot\boldsymbol{\nabla}\boldsymbol{u} = -\frac{\boldsymbol{\nabla} P}{\rho} \underbrace{-2(\boldsymbol{\Omega_p} + \boldsymbol{\Omega_c}) \times \boldsymbol{u}}_{\text{Coriolis force } \boldsymbol{F_c}} \underbrace{-(\boldsymbol{\Omega}_\mathrm{p} \times \boldsymbol{\Omega_c}) \times \boldsymbol{r}}_{\text{Poincaré force } \boldsymbol{F_p}} + \nu\nabla^2\boldsymbol{u}. \tag{1}$$

comprises, as indicated, a Coriolis and a Poincaré force term. Here, $\boldsymbol{u}$ is the velocity field (supposed to be divergence-free), P a modified pressure (that includes also centrifugal terms), $\boldsymbol{\Omega}_p$ the precession angular frequency, $\boldsymbol{\Omega}_c$ the angular frequency of the container, and ν the kinematic viscosity of the fluid [77]. In the container frame, the boundary conditions at all walls are no-slip.

Denoting by α the nutation angle between the rotation and the precession axis (see Figure 2 (a)), $\boldsymbol{\Omega}_\mathrm{p}$ in the container frame reads

$$\boldsymbol{\Omega}_p(t) = \Omega_p\big[\sin\alpha\cos(\Omega_c t+\varphi)\widehat{\boldsymbol{r}} - \sin\alpha\sin(\Omega_c t+\varphi)\widehat{\boldsymbol{\varphi}} + \cos\alpha\widehat{\boldsymbol{z}}\big], \tag{2}$$

with $\widehat{\boldsymbol{r}}$, $\widehat{\boldsymbol{\varphi}}$, and $\widehat{\boldsymbol{z}}$ being the unit vectors in radial, azimuthal, and axial direction, respectively.

Then, the Poincaré force in equation (1), which results from the temporal change of the orientation of the rotation axis, acquires the form

$$\boldsymbol{F}_p = -\Omega_c\Omega_p r\sin\alpha\cos(\Omega_c t+\varphi)\widehat{\boldsymbol{z}}\,. \tag{3}$$

The spatial structure of this Poincaré force preordains the fundamental pattern of the directly driven flow which consists of a non-axisymmetric mode with azimuthal wave number $m = 1$ ($\propto \cos\varphi$) and axial wave number $k = 1$, representing a flow that is anti-symmetric with respect to the equatorial plane (Figure 2 (b), middle).

For a more general characterization of precession driven flows in cylinders with height H and radius R it is most appropriate to use the eigenfunctions (inertial waves), resulting from the linear inviscid approximation of rotating systems, which have the analytical form

$$\boldsymbol{U}_j(r,z,\varphi,t) = \boldsymbol{u}_j(r,z)e^{\mathrm{i}(\omega_j t+m\varphi)} + \text{c.c.}\,. \tag{4}$$

Here, the collective index j incorporates three integers m,k,n, comprising the azimuthal wave number m and the axial wave number k. A third (radial) number n counts the roots of the dispersion relation

$$\omega_j\zeta_j \mathrm{J}_{m-1}(\zeta_j) + m\big(2-\omega_j\big)\mathrm{J}_m(\zeta_j) = 0 \qquad \text{with} \qquad \omega_j = \pm 2\left[1+\left(\frac{\zeta_j}{\Gamma k\pi}\right)^2\right]^{-1/2}, \tag{5}$$

that determines the eigenfrequences of the inertial modes. In Equation (5), J_m denotes the Bessel function of order m, Γ the aspect ratio defined by $\Gamma := H/R$, and ζ_j a radial wave number with its position in the sequence of zeros of (5) corresponding to the number of half-cycles in the radial

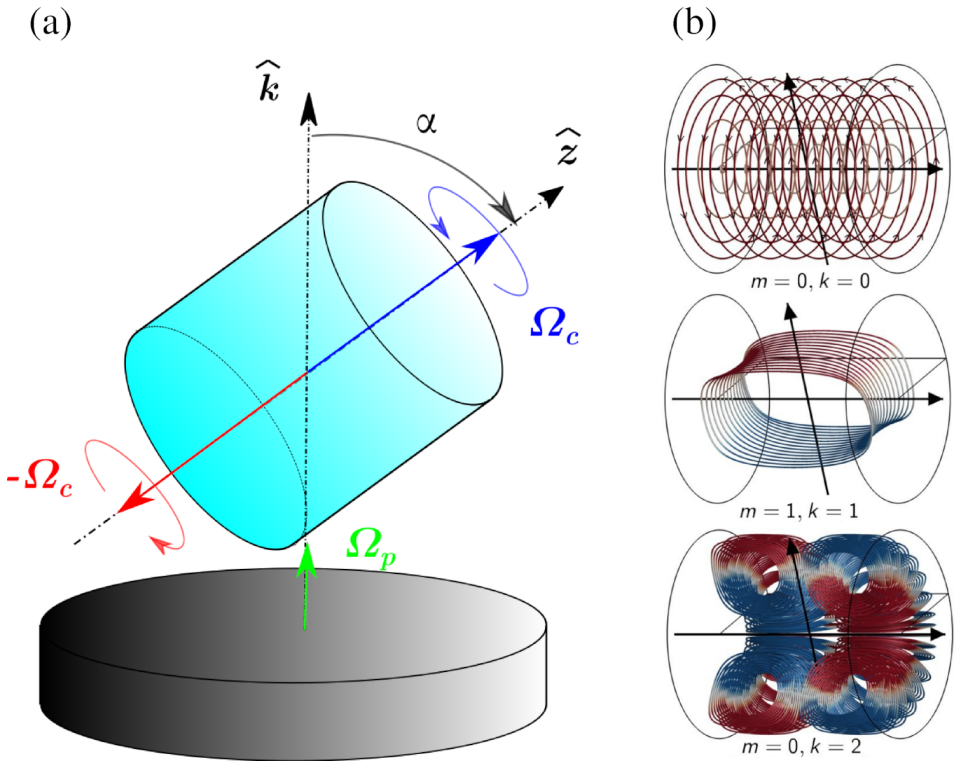

Figure 2. (a) Sketch of a precessing cylinder with the container's angular frequency $\Omega_c = 2\pi f_c$ and the precession angular frequency $\Omega_p = 2\pi f_p$. The nutation angle α between the axis of precession $\widehat{\boldsymbol{k}}$ and the axis of rotation $\widehat{\boldsymbol{z}}$ varies between 0 and 90°. Pro- and retrograde precession is indicated in blue and red, respectively. (b) The three most important flow modes are (from top to bottom): the geostrophic, axisymmetric mode with $(m = 0, k = 0)$; the forced mode with $(m = 1, k = 1)$, and the axisymmetric double-roll mode with $(m = 0, k = 2)$.

direction. For the following it is important that an inertial mode becomes resonant when the frequency of the precession matches the natural frequency of a corresponding eigenfunction. For the resonance of the simplest inertial (or Kelvin) mode with $m = 1$, $k = 1$ and $n = 1$, this condition applies to the aspect ratio $\Gamma = 1.9898$, which is indeed very close to the value $\Gamma = 2$ chosen for the DRESDYN experiment.

Going beyond the linear regime, for increasing forcing the nonlinear interactions of the forced mode with itself, and with its viscous modifications in the boundary layers, become relevant. The underlying nonlinear theory is a quite complex issue and allows for closed solutions only under special conditions in the weakly nonlinear regime [78–80]. One of the major flow contributions beyond the directly forced mode is connected with a considerable modification of the azimuthal circulation [59,81] that is always oriented opposite to the (initial) solid body rotation, giving rise to a "braking" of the flow in the bulk of the cylinder. A direct consequence of the reduced rotation is the observed detuning [82–85] of free inertial modes that emerge in form of triadic resonances [86,87]. For very strong forcing, the rotation profile even becomes Rayleigh-unstable, leading to an abrupt transition into a turbulent flow regime, which also shows a hysteretic behaviour [63].

2.2. *Numerics*

Having discussed the basic physics of precession-driven flows in the container frame, we turn now to the numerical simulations that were actually carried out in the so-called *turntable frame*. In this frame, the Poincaré force vanishes and the boundary conditions are governed by the cylinder walls rotating at Ω_c. We used the spectral element Fourier code *Semtex* [88], and meshed the domain with 300 quadrilateral elements in the meridional half plane and 128 Fourier modes in azimuthal direction.

As for the magnetic field, we focus on the kinematic dynamo problem and solve the corresponding induction equation in a fluid with conductivity σ

$$\frac{\partial \boldsymbol{B}}{\partial t} = \boldsymbol{\nabla} \times \left(\langle \boldsymbol{u} \rangle \times \boldsymbol{B} - \frac{\nabla \times \boldsymbol{B}}{\mu_0 \sigma} \right) \tag{6}$$

for the resulting time-averaged velocity field $\langle \boldsymbol{u} \rangle$ by means of a finite volume method with constraint transport which maintains the divergence-free condition $\nabla \cdot \boldsymbol{B} = 0$. While, in principle, the code developed in [89] allows a correct treatment of vacuum boundary conditions by employing an additional surface integral equation, for our quite comprehensive parameter studies we employed the simplified vertical-field conditions by demanding all tangential field components to vanish at the surface. Comparable studies, as previously applied to other dynamo experiments [90–92], showed that vertical-field conditions typically lead to somewhat lower thresholds for the occurrence of dynamo action when compared to more realistic vacuum boundary conditions. Corresponding comparisons for the DRESDYN experiment are ongoing and will be published elsewhere.

Specifically, the simulations were carried out as follows: at $t = 0$ we started with a pure solid body rotation, which in the turntable frame reads $\boldsymbol{u} = (\Omega_c r)\widehat{\boldsymbol{\varphi}}$. Then we imposed the precessional forcing, and waited until the flow had reached a statistically steady regime. After inserting the resulting time-averaged flow field $\langle \boldsymbol{u} \rangle$ into the induction equation (6), the kinematic dynamo simulations were run for more than one diffusion time, after which an exponential growth, or decay, is clearly established. As we will see later, dynamo action mainly occurs in the transition regime (between the laminar and the fully turbulent regime) which is governed by only a few large-scale modes. Here, the utilized time-averaged flow can be considered as a good representative of the total flow.

The typical parameter space investigated numerically for the kinematic dynamo problem covers Reynolds numbers $Re := R^2|\Omega_c + \Omega_p \cos\alpha|/\nu \in [1000, 10000]$ and precession ratios (or Poincaré numbers) $Po := \Omega_p/\Omega_c \in \pm\,[0.01, 0.20]$. Later on, we will focus on the results for nutation angles $\alpha = 75°$, both for prograde and retrograde precession, as well as for $\alpha = 90°$.

2.3. *The* 1 : 6 *down-scaled water experiment*

Complementary to the numerical simulations, we have set-up and utilized a water experiment, which is 1 : 6 down-scaled with respect to the big machine, to measure the flow structure and amplitude (Figure 3). This device consists of a cylindrical vessel with inner height $H = 326$ mm and inner radius of $R = 163$ mm. Just as the big one, the down-scaled vessel can rotate with a maximum rotation rate of 10 Hz around its axis, while the turntable can rotate with up to 1 Hz. One end wall of the vessel is equipped with 9 ultrasound transducers (TR0408SS, Signal Processing SA, Lausanne), six of which being arranged in a radial array ranging from $r/R = 0$ to 0.92. Four transducers are located at $r/R = 0.92$ (i.e., $r = 150$ mm), with 90° azimuthal spacing in order to estimate the azimuthal symmetry of the flow. All transducers are aligned parallel to the vessel axis and can capture the instantaneous axial velocity distribution between $z/H = 0$ and 1. The transducers are connected to an ultrasound Doppler velocimeter (DOP 3010, Signal

Processing SA, Savigny) that records the velocity profiles with a temporal resolution of about 10 Hz.

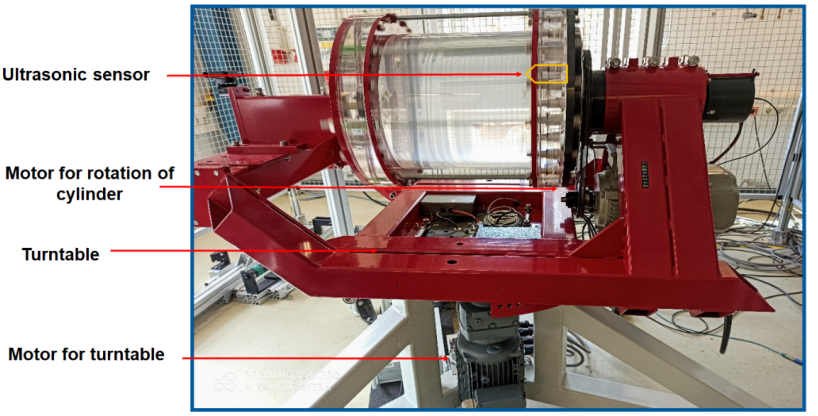

Figure 3. The 1 : 6 down-scaled water precession experiment with the central vessel of radius $R = 163$ mm and height $H = 326$ mm. The nutation angle can vary between 60° and 90°.

Later below, we will show measurements with one ultrasonic transducer at radius $r = 150$ mm. During the experiments, the room was air-conditioned in order to minimize any changes of the temperature-dependent viscosity of water (assumed as $\nu = 1 \times 10^{-6}\mathrm{m}^2\mathrm{s}^{-1}$).

2.4. *Comparison between numerical and experimental results*

In the following, we will summarize and compare some of the most important numerical and experimental results, with the main focus on the flow dependence on the precession ratio Po and the nutation angle α. As for the latter, we will concentrate on the exemplary cases 75° prograde, 90° and 75° retrograde (more results can be found in [93–95]). Figure 4 shows the temporal evolution of the depth dependence of the axial velocity profile u_z, as measured by one UDV sensor at $r = 150$ mm (the depth indicates the distance along the beam axis from the transducer). The three rows display results for $\alpha = 75°$ prograde, 90° and $\alpha = 75°$ retrograde. The visible oscillatory pattern of the velocity profile (governed by the rotational frequency Ω_c of the cylinder to which the sensor is attached) is representative of the directly forced $(m = 1, k = 1)$ mode which is stationary in the turntable frame.

With growing Po we observe, for all considered angles, an increasingly complex flow pattern. At lower values of Po (first column), the flow shows a stable structure which is mirrored by the regular pattern in form of vertical stripes in all cases. As Po exceeds a certain higher value, for $\alpha = 75°$ prograde and 90° the flow structure changes and exhibits a breaking of the equatorial symmetry, as evidenced by the emerging tilt of the stripes. By contrast, in the 75° retrograde case (third row) the occurrence of the tilt is shifted to larger values of Po.

This breaking of the equatorial symmetry indicates a flow state transition at a critical value of Po, where Kelvin modes with even axial wave numbers emerge [93]. This transition has considerable effects on the amplitudes of all flow modes, which we will quantify in the following.

The mode amplitudes are calculated by decomposing the axial velocity field $u_z = u_z(r, \varphi, z, t)$ into (m, k) modes (the details of the underlying discrete sine transformation can be found in [95]). Of the various observable modes, we mainly examined those which acquire substantial

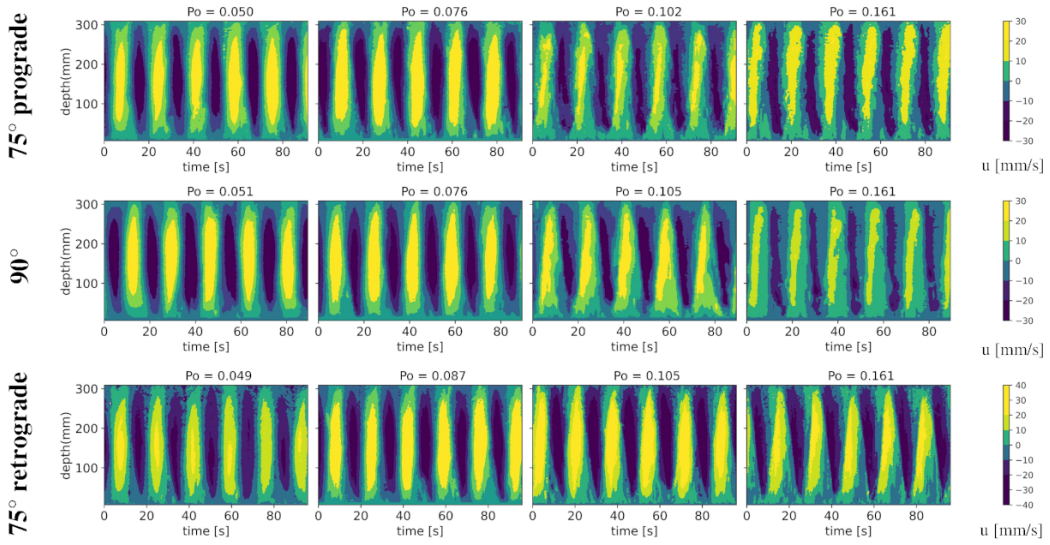

Figure 4. Axial velocity u_z, measured by one UDV sensor positioned at $r = 150$ mm, in dependence on time and depth, for three different nutation angles and four different Po. The Reynolds number in all cases was approximately 10^4. Adapted from reference [95].

amplitudes and are most relevant for dynamo action [74]. This applies, in particular, to the directly forced ($m = 1, k = 1$) mode and the torus-shaped ($m = 0, k = 2$) mode (see Figure 2 (b)).

Figure 5 shows the measured and simulated amplitudes of these prominent modes versus the precession ratio Po for the three angles 75° prograde, 90°, and 75° retrograde, respectively. Note that, since a comprehensive numerical parameter sweep at $Re \approx 10^4$ would have been forbiddingly expensive, the results of simulations carried out at $Re = 6500$ were linearly extrapolated to the higher experimental value $Re = 10^4$ (while, in this low Re regime, the scaling of the mode amplitudes might actually be a bit flatter then linear, any arising discrepancies remain rather small).

For 75° prograde and 90°, we observe that the directly forced ($m = 1, k = 1$) mode increases up to $Po \approx 0.08$, beyond which there is an abrupt transition of the flow state connected with a breakdown of this mode. Simultaneously, an axially symmetric mode ($m = 0, k = 2$) emerges in a narrow range of Po, which corresponds to the double-roll structure that was previously shown to be most relevant for dynamo action [93]. Obviously, the nutation angle influences the critical Po, such that as the angle increases (from 75° prograde to 90°), so does the critical Po (from 0.087 to 0.10).

By contrast, the data for 75° retrograde precession exhibit not such a clear breakdown of the directly forced ($m = 1, k = 1$) mode whose amplitude rather shows a gradual decrease with Po. At the same time, we observe a smoother increase of the axially symmetric ($m, = 0, k = 2$) mode within the considered range of Po. In comparison to the other cases, $\alpha = 75°$ retrograde exhibits the largest amplitude of the ($m = 0, k = 2$) mode, and the critical Po is shifted to larger values. In general, the results of the numerical simulations are in good agreement with the experimental values, with the exception of the ($m = 0, k = 2$) mode for the case 75° prograde when Po is large. The latter discrepancy is presently not well understood.

The right column of Figure 5 may help to explain the observed transitions. It shows, for the three nutation angles, the radial profile of the angular momentum $L(r) = r u_\varphi(r)$, averaged both in azimuthal and axial direction (excluding the boundary layers at the endcaps). For all α, with increasing Po the angular momentum deviates more and more from the original solid

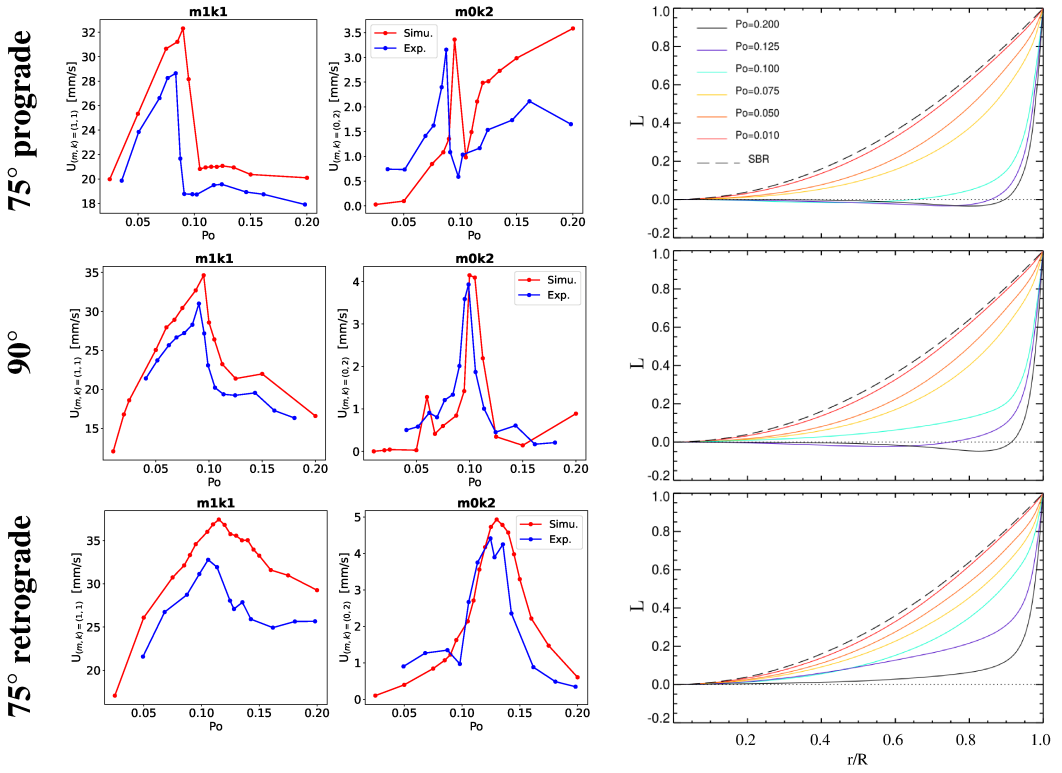

Figure 5. Left: Comparison of the amplitudes of the directly forced ($m = 1, k = 1$) mode and the axisymmetric ($m = 0, k = 2$) mode between numerically calculated (red) and experimentally measured flows (blue) for three representative nutation angles. Note that the numerical values were computed at $Re = 6500$ and then (linearly) extrapolated to the experimental value $Re = 10000$. Adapted from reference [95]. Right: Radial distribution of the (normalized) angular momentum, determined numerically at $Re = 6500$, for the three considered angles. Adapted from reference [94].

body rotation (SBR) and eventually becomes rather flat, at least until $r/R < 0.8$, say. Remarkably, though, for 75° prograde and 90°, L turns slightly negative, indicating a *counter-rotation* in this region, and a breaking of Rayleigh's stability criterion (radially increasing L^2). By contrast, this breaking of the Rayleigh criterion does not occur for 75° retrograde, which might explain the smoother transition in this case. However, the violation of the Rayleigh criterion occurs only (appr. 15 per cent) after the onset of instability, suggesting that a complete understanding of this connection would also require to consider the influence of large-scale radial and axial flow components (a quantitative improvement might also result when measuring the angular momentum in the frame of inertia rather than in the turntable frame as done here).

2.5. *Towards an optimized dynamo*

Based on the rather consistent experimental and numerical findings of the last subsection, we ask now what Poincaré number and nutation angle might be best suited for dynamo action. The relevant criterion is a minimum value of the critical magnetic Reynolds number $Rm = RePm$ (with the magnetic Prandtl number $Pm = \mu_0 \sigma \nu$). Self-excitation is characterized by an

exponential increase of the volume-averaged magnetic energy when time-stepping the induction equation (6). From the temporal evolution of the magnetic energy the growth rate γ is calculated.

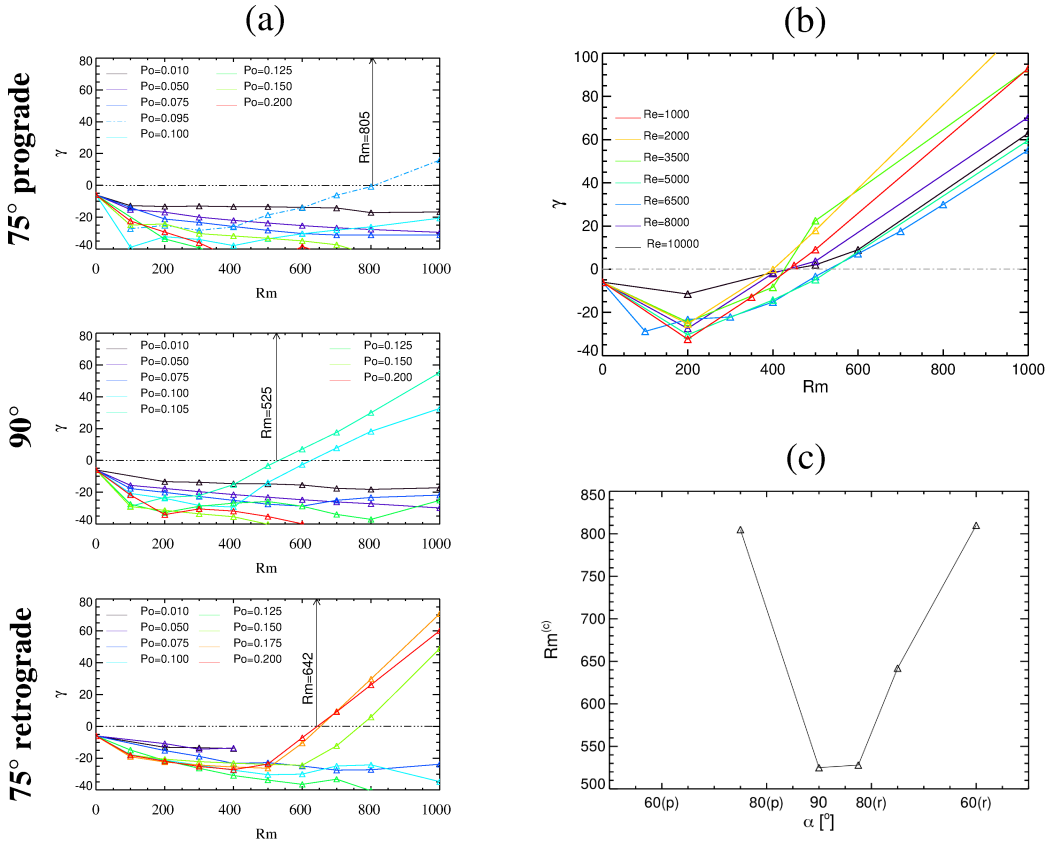

Figure 6. (a) Growth rate γ of the magnetic field energy as a function of the magnetic Reynolds number $Rm = RePm$ for three nutation angles α, computed at $Re = 6500$. The different curves represent different precession ratios, and the arrows mark the dynamo onset at the optimum Po characterized by the lowest critical Rm. (b) Dependence of the lowest critical Rm on Re for the special case $\alpha = 90°$. Note the decrease of the critical Rm from 525 (for $Re = 6500$) to 430 (for $Re = 10000$), in agreement with [74]. (c) Dependence of the optimized critical Rm on the nutation angle α, simulated for $Re = 6500$. The optimum α seems to lie somewhere between 90° and 82.5° retrograde. (a) and (b) are adapted from Reference [95]. (c) is adapted from [96].

In Figure 6 (a), we plot the Rm-dependence of γ for eight different precession ratios Po, and a fixed $Re = 6500$. The critical Rm achieves a minimum of 525 for $Po = 0.1$ and $\alpha = 90°$. For this particular angle, Figure 6 (b) specifies the Rm-dependence of γ when computed for different values of Re. We observe a sort of convergence to a critical Rm of 430, which had already been found in [74,93]. However, as shown in Figure 6 (c), the real optimum might still lie at slightly retrograde precession, somewhere between 90° and 82.5°. It is this range of nutation angles where we will start our hunt for dynamo action. As for Po, we will focus on the transition region with a strong contribution of the $(m = 0, k = 2)$ mode, which for high Re seems to converge to a Po value between 0.06 and 0.07 [63,93]. Note, however, that beyond the transition region, i.e. in the fully turbulent regime, the use of the time-averaged velocity field in the induction equation

becomes increasingly problematic. Dynamo simulations for the time-dependent flow fields in this regime are underway and will be published elsewhere.

3. The machine

Following up on the pioneering experiments in Riga, Karlsruhe and Cadarache, the DRESDYN precession experiment (Figure 7) is supposed to work as a truly homogeneous dynamo that does not use any impellers, guiding tubes, or magnetic materials (for the two other recent experimental efforts in Maryland and Madison with a similar ambition, see [97] and [98], respectively.) The central rotation vessel encases a cylindrical sodium volume of 2 m diameter and 2 m height (Figure 8). This size resulted as a sort of optimum from the two requirements to reach a magnetic Reynolds number of about 700 while keeping the necessary driving power (which scales, in the turbulent regime, as $\sim Rm^3/R$) in the technically affordable range of 1 MW. While the latter value can be roughly estimated from extrapolating the 10 W jump as measured in the downscaled water experiment at 4 Hz (see [63, Figure 4]) it certainly needs real confirmation in the "big one". For this vessel, we aim at reaching a rotation rate of 10 Hz to obtain $Rm = 700$, and a precession rate of 1 Hz to cover the laminar, the fully turbulent, and the transition state in between them which is the most "dynamo-prone" one. This motion of the vessel, which is driven by a motor with maximum electric power of 1.2×10^6 Watts, results in an acceleration of 500 g and a total gyroscopic torque of up to 8×10^6 Nm. The total budget of moving masses amounts to approximately 150 tons. From a mechanical perspective, the entire machine is in many respects at the edge of technical feasibility, so that a careful design and much optimization was required to ensure that the mechanical strain does not exceed the material limitations [99].

Due to the use of sodium (the best liquid conductor) and the high acceleration forces, critical components had to be developed and manufactured in-house. In addition to the mechanical challenges, this also included the design and implementation of both a personal safety system (PSS) and a machine interlock system. Here, the real-time extraction of internal states for machine-monitoring and an online camera inspection of the container surface had to be implemented. As this involves the use of FFT-transforms, a sampling rate of 6 kHz was selected for all sensors in the data acquisition system (DAQ). On the other side, this also ensures a high level of qualitative and quantitative data recording on both platform and vessel in order to answer the scientific questions posed to the experiment. To withstand the exceptional conditions (120°C, accelerations up to 500 g), commercially available DAQ-electronics were not qualified, so that a dedicated DAQ-system had to be developed and tested in-house. The communication between the sensor electronics on the vessel and the evaluation system is based on ethernet, providing sufficient bandwidth to transfer data via two signal rotary transmitters (for the container and the platform), in order to enable live processing and viewing of the measurement data.

The simultaneous rotation around two axes poses a couple of challenges for the filling and emptying procedures, heating and the handling of thermal expansion of sodium. To accommodate all resulting requirements, a decision was made in favor of a slightly enlarged vessel (Figure 8), comprising two conical volumes that serve, first, for a well-defined filling and emptying procedure at 43° vessel tilting, and, second, for hosting two bellows which will compensate the thermal expansion of the liquid sodium.

For the vessel material the austenitic steel 1.4571 was chosen which is well-known for its corrosion resistance against liquid sodium. A shell thickness of 3 cm makes it safe to withstand the centrifugal pressure of approximately 20 bar in case of pure rotation with 10 Hz. While for increasing precession ratio this total pressure decreases, it is complemented by an increasing pressure vacillation Δp of up to 10 bar, resulting from the gyroscopic forces (see [100, Figure 1]). In addition to those mechanical stresses, we also had to consider thermal stresses caused by

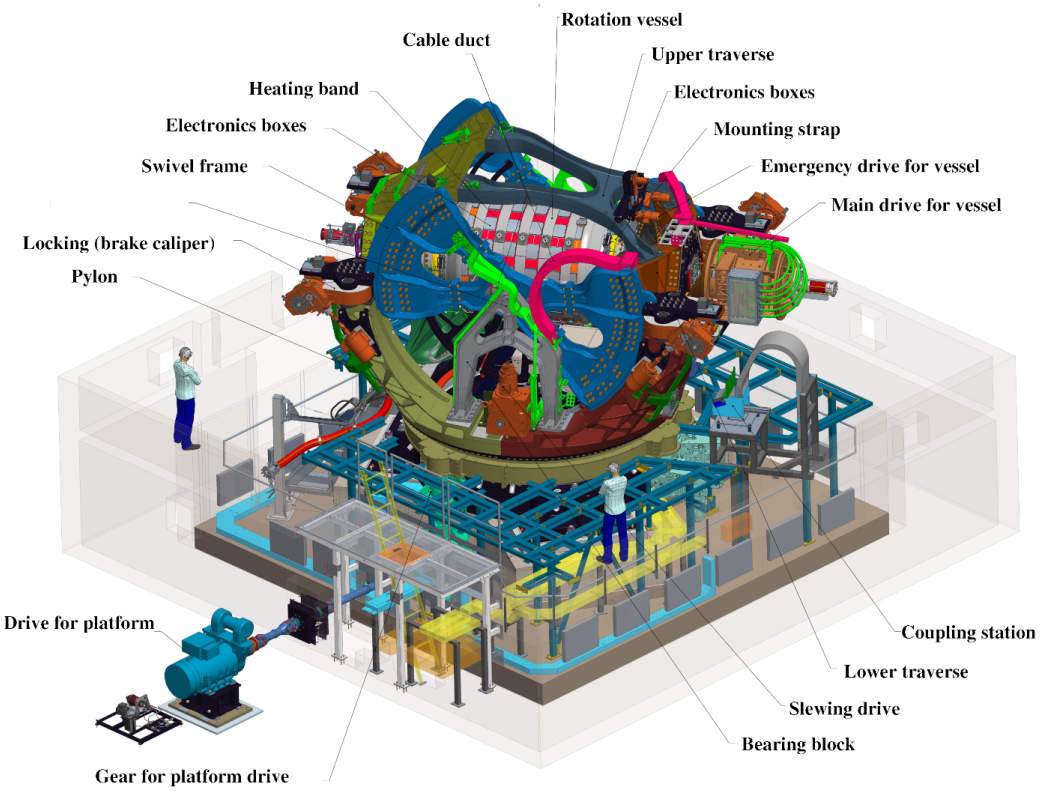

Figure 7. Drawing of the DRESDYN precession experiment with main parts indicated. The separate basement rests on 7 ferro-concrete pillars reaching 22 m deep into the bedrock. The machine is housed in a containment (the lower part of which being indicated in gray). The 540 kW drive for the platform is situated in a separate engine room, jointly with the two oil lubrication systems for the large slewing bearing and the two bearings for the rotation vessel.

the temperature difference over the shell when the rotating vessel is cooled by a strong flow of air [101].

Speaking of temperature: any attempt at perfectly controlling it, i.e. by using an oil jacket as in the Maryland experiment [97], would have required an enormous technical effort. Presently, cooling is realized by a strong air flow in the containment which provides (through the 3 cm stainless-steel wall of the vessel) a cooling power of around 50 kW. Heating before the experiment, and between the runs, is accomplished by heating foils with a total power of appr. 60 kW. In view of the vast thermal inertia of the sodium and the vessel, these cooling and heating processes would lead to temperature ramps of appr. 0.2 degree per minute which seem well manageable by a thorough protocol of the experimental campaign. The big player, though, is the expected hydrodynamic dissipation, going up to 1 MW in the fully turbulent regime, which indeed constrains the duration of individual runs.

Although the main goal of the experiment is to achieve dynamo action in a truly homogeneous volume, we have also provided some baffles at the end caps which can be inserted into the cylindrical volume. By increasing the penetration depth of the baffles, the flow transitions are shifted to larger Poincaré numbers [102]. This gives, on one hand, an additional handle to further optimize the dynamo conditions, but may, on the other hand, also help to elucidate the role of topographic roughness on the transport of angular momentum in rapidly rotating fluids [103].

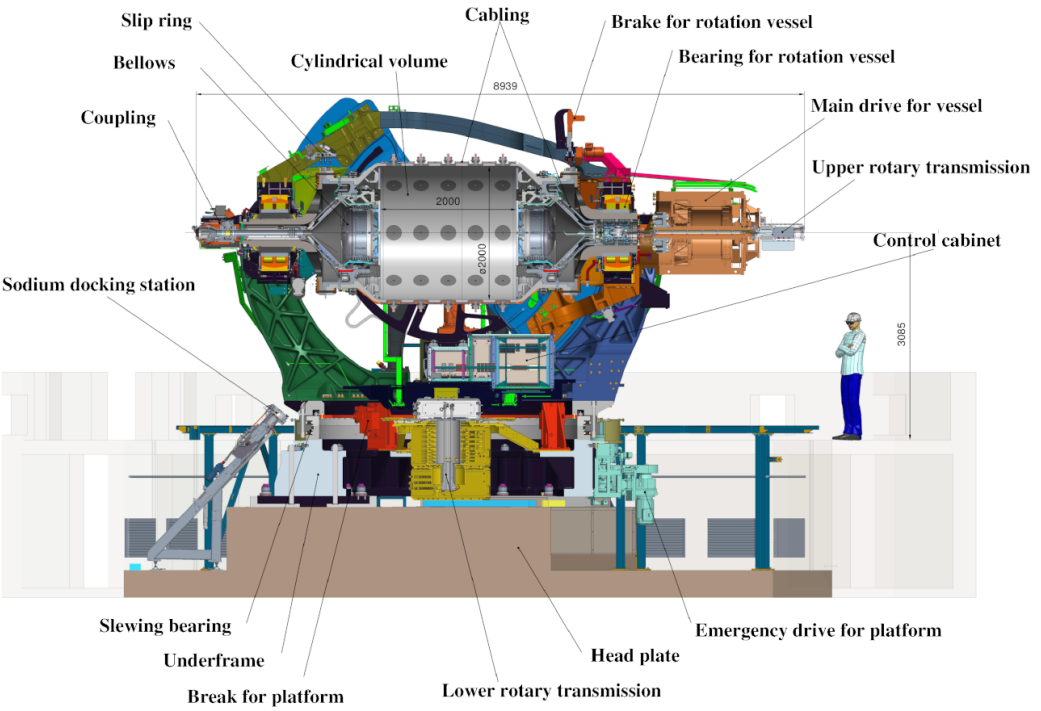

Figure 8. Sectional view of the DRESDYN precession experiment with the main dimensions indicated (in mm).

A particular challenge was the design of the tilting frame that allows to choose different angles between rotation and precession axis. Finding appropriate roller bearings for the vessel turned out to be quite demanding, mainly because of the huge gyroscopic torque. The same gyroscopic torque also requires a very stable basement, supported by seven pillars, each extending into the granite bedrock. For safety measures, the entire machine is housed in a containment. Since the double rotation cannot be stopped quickly in case of an accident, this containment is the only chance of preventing sodium jets (when spilling out of a potential leak) from covering all surrounding areas. For such accidents, the containment can be flooded with argon, which is stored in liquid form. A corresponding test has validated that by injecting 4 tons of argon the oxygen content in the containment can be reduced to 4 per cent which is low enough for extinguishing any sodium fire [104].

After many years of design and construction (see Figure 9 (a-c)), the “marriage” between the frame and the vessel was successfully carried out on 17 January 2024 (Figure 9 (d, e)). After accomplishing some remaining technical work, first precession experiments with water are scheduled for fall 2024. In these experiments, the flow diagnostics will mainly rely on the data of pressure sensors (situated in the flanges of the vessel) whose amplitudes and spatial structures can be matched to the typical flow modes discussed above. Some tests with UDV sensors are also foreseen, but will presumably be restricted to lower rotation rates when the velocities and the centrifugal accelerations are not too excessive. For the later sodium experiments, two rows of flanges will be equipped with Hall sensors to measure the magnetic field.

Figure 9. Some impressions from the construction, with relevant dates indicated. (a) Shell construction of the containment and the air duct (for cooling). (b) Insertion of the underframe. (c) Slewing bearing mounted on the underframe. (d) and (e) Insertion of the vessel into the frame. (f) The DRESDYN building.

4. Conclusion

Besides the 3 m diameter spherical Couette experiment in Maryland [97] and the 3 m diameter Madison plasma dynamo experiment (MPDX) [98], the DRESDYN precession experiment is another attempt to realize a truly homogeneous dynamo in the lab. Setting into motion a cylindrical volume of liquid sodium by two rotations, dynamo action is expected to start at a magnetic Reynolds number of around 430, a precession ratio of approximately 0.06, and a nutation axis close to 90°. For these parameters we expect a dynamo-prone flow state, governed by a combination of differential rotation, a remaining $(m = 1, k = 1)$ mode, and a double-roll mode of the $(m = 0, k = 2)$-type. Since this flow combination is not yet strongly turbulent, we do not expect any significant turbulence-enhanced resistivity which might have played (possibly) a detrimental role in previous dynamo experiments [105].

While we have little doubt that the flow state in the big machine will be quite similar to that extrapolated from numerical simulations and the results of the 1 : 6 down-scaled water experiment, there are some remaining caveats concerning the role of the magnetic boundary conditions on dynamo action. First water experiments, which are expected still for 2024, will be decisive in validating the mechanical integrity of the entire machine with respect to the huge mechanical loads resulting from the gyroscopic moment. Moreover, these water experiments will allow to validate the flow predictions based on previous numerical and experimental results, and to further constrain the optimal conditions for dynamo action. If everything runs smoothly, first sodium experiments may start in 2025, provided that the technical inspection of the rotation vessel after the water experiments does not reveal any structural failures. Apart from its specific goal to show self-excitation in a mechanically forced homogeneous fluid, we also hope that this experiment may act as a catalyst for further investigations into astronomical forcings of planetary and stellar dynamos.

Acknowledgments

We would like to thank Oliver Bähr, Martin Becker, Andre Büchner, Jürgen Claussner, Thomas Egeln, Hans-Olaf Engel, Johannes Feder, Tim Gitzel, Jonas Gorgis, Stefan Grunze, Jens Helbig, Frank Herbrand, Jakob Kaiser, Richard Kaubisch, Sebastian Köppen, Bert Lange, Markus Meyer, Benjamin Nebe, Pierre Ramm, Anett Schräger, Robert Stöckel, Thomas Süßmilch, Henrik Tietze, Thomas Wiesner, Bernd Wustmann, and Yvonne Zimmermann for technical support, and Johan Herault and Thomas Albrecht for early contributions to the project. The long-lasting cooperation with Georg Schnurr, Gunter Weigelt and Steffen Wohlrab from SBS Bühnentechnik Dresden, and with Michael Beitelschmidt and Stephan Rother from TU Dresden is gratefully acknowledged.

Declaration of interests

The authors do not work for, advise, own shares in, or receive funds from any organization that could benefit from this article, and have declared no affiliations other than their research organizations.

References

[1] H. K. Moffatt and E. Dormy, *Self-exciting fluid dynamos*, Cambridge Texts in Applied Mathematics, Cambridge University Press: Cambridge, 2019.
[2] F. Rincon, "Dynamo theories", *J. Plasma Phys.* **85** (2019), article no. 205850401.
[3] S. Tobias, "The turbulent dynamo", *J. Fluid Mech.* **912** (2021), article no. P1.
[4] A. Gailitis, O. Lielausis, E. Platacis, G. Gerbeth and F. Stefani, "*Colloquium:* Laboratory experiments on hydromagnetic dynamos", *Rev. Mod. Phys.* **74** (2002), pp. 973–990.
[5] F. Stefani, A. Gailitis and G. Gerbeth, "Magnetohydrodynamic experiments on cosmic magnetic fields", *Z. Angew. Math. Mech.* **88** (2008), pp. 930–954.
[6] G. Verhille, N. Plihon, M. Bourgoin, P. P. Odier and J.-F. Pinton, "Laboratory dynamo experiments", *Space Sci. Rev.* **152** (2010), pp. 543–564.
[7] D. P. Lathrop and C. B. Forest, "Magnetic dynamos in the lab", *Phys. Today* **64** (2011), pp. 40–45.
[8] F. Stefani, "Liquid metal experiments on geophysical and astrophysical phenomena", *Nat. Rev. Phys.* **6** (2024), pp. 409–425.
[9] Y. B. Ponomarenko, "On the theory of hydromagnetic dynamos", *Zh. Prikl. Mekh. & Tekh. Fiz. (USSR)* **6** (1973), pp. 47–51.
[10] A. Gailitis, O. Lielausis, S. Dement'ev, et al., "Detection of a flow induced magnetic field eigenmode in the Riga dynamo facility", *Phys. Rev. Lett.* **84** (2000), pp. 4365–4368.
[11] A. Gailitis, O. Lielausis, E. Platacis, et al., "Magnetic field saturation in the Riga dynamo experiment", *Phys. Rev. Lett.* **86** (2000), pp. 3024–3027.

[12] A. Gailitis, O. Lielausis, E. Platacis, G. Gerbeth and F. Stefani, "The Riga dynamo experiment", *Surv. Geophys.* **24** (2003), pp. 247–267.

[13] A. Gailitis, O. Lielausis, E. Platacis, G. Gerbeth and F. Stefani, "Riga dynamo experiment and its theoretical background", *Phys. Plasmas* **11** (2004), pp. 2838–2834.

[14] A. Gailitis, G. Gerbeth, T. Gundrum, O. Lielausis, G. Lipsbergs, E. Platacis and F. Stefani, "Self-excitation in a helical liquid metal flow: the Riga dynamo experiments", *J. Plasma Phys.* **84** (2018), article no. 73584030.

[15] U. Müller and R. Stieglitz, "The Karlsruhe dynamo experiment", *Nonl. Proc. Geophys.* **9** (2002), pp. 165–170.

[16] U. Müller, R. Stieglitz and S. Horanyi, "A two-scale hydromagnetic dynamo experiment", *J. Fluid Mech.* **498** (2004), pp. 31–71.

[17] U. Müller, R. Stieglitz and S. Horanyi, "Experiments at a two-scale dynamo test facility", *J. Fluid Mech.* **552** (2006), pp. 419–440.

[18] U. Müller and R. Stieglitz, "The response of a two-scale kinematic dynamo to periodic flow forcing", *Phys. Fluids* **21** (2009), article no. 034108.

[19] R. Monchaux, M. Berhanu, M. Bourgoin, et al., "Generation of a magnetic field by dynamo action in a turbulent flow of liquid sodium", *Phys. Rev. Lett.* **98** (2007), article no. 044502.

[20] M. Berhanu, R. Monchaux, S. Fauve, et al., "Magnetic field reversals in an experimental turbulent dynamo", *Eur. Phys. Lett.* **77** (2007), article no. 59001.

[21] F. Ravelet, M. Berhanu, R. Monchaux, et al., "Chaotic dynamos generated by a turbulent flow of liquid sodium", *Phys. Rev. Lett.* **101** (2008), article no. 074502.

[22] R. Monchaux, M. Berhanu, S. Aumaître, et al., "The von Kármán sodium experiment: Turbulent dynamical dynamos", *Phys. Fluids* **21** (2009), article no. 035108.

[23] B. Gallet, S. Aumaître, J. Boisson, et al., "Experimental observation of spatially localized dynamo magnetic fields", *Phys. Rev. Lett.* **108** (2012), article no. 144501.

[24] A. Giesecke, F. Stefani and G. Gerbeth, "Role of soft-iron impellers on the mode selection in the von-Kármán-sodium dynamo experiment", *Phys. Rev. Lett.* **104** (2010), article no. 044503.

[25] S. Kreuzahler, Y. Ponty, N. Plihon, H. Homann and R. Grauer, "Dynamo enhancement and mode selection triggered by high magnetic permeability", *Phys. Rev. Lett.* **119** (2017), article no. 234501.

[26] C. Nore, D. C. Quiroz, L. Cappanera and J.-L. Guermond, "Numerical simulation of the von-Kármán-sodium dynamo experiment", *J. Fluid Mech.* **854** (2018), pp. 164–195.

[27] F. Stefani, G. Gerbeth, U. Günther and M. Xu, "Why dynamos are prone to reversals", *Earth Planet. Sci. Lett.* **243** (2006), pp. 828–840.

[28] F. Pétrélis, S. Fauve, E. Dormy and J.-P. Valet, "Simple mechanism for reversals of Earth's magnetic field", *Phys. Rev. Lett.* **102** (2009), article no. 144503.

[29] R. Benzi and J.-F. Pinton, "Magnetic reversals in a simple model of magnetohydrodynamics", *Phys. Rev. Lett.* **105** (2010), article no. 024501.

[30] M. Le Bars, D. Cébron and P. Le Gal, "Flows driven by libration, precession, and tides", *Annu. Rev. Fluid Mech.* **147** (2015), pp. 163–193.

[31] G. Consolini and P. De Michelis, "Stochastic resonance in geomagnetic polarity reversals", *Phys. Rev. Lett.* **90** (2003), article no. 058501.

[32] M. Fischer, G. Gerbeth, A. Giesecke and F. Stefani, "Inferring basic parameters of the geodynamo from sequences of polarity reversals", *Inverse Probl.* **25** (2008), article no. 065011.

[33] L. Cappellotto, M. J. Orgeira, V. M. V. Herrera and R. G. Cionco, "Multivariable statistical analysis between geomagnetic field, climate, and orbital periodicities over the last 500 kyr, and their relationships during the last interglacial", *Global Planet. Change* **213** (2022), article no. 103836.

[34] M. Landeau, A. Fournier, H.-C. Nataf, D. Cebron and N. Schaeffer, "Sustaining Earth's magnetic dynamo", *Nat. Rev. Earth Environ.* **3** (2022), pp. 255–269.

[35] C. A. Dwyer, D. J. Stevenson and F. Nimmo, "A long-lived lunar dynamo driven by continuous mechanical stirring", *Nature* **479** (2011), pp. 212–214.

[36] S. M. Tikoo, B. P. Weiss, D. L. Shuster, C. Suavet, H. Wang and T. L. Grove, "A two-billion-year history for the lunar dynamo", *Sci. Adv.* **3** (2017), article no. e170020.

[37] R. R. Fu, B. P. Weiss, D. L. Shuster, et al., "An ancient core dynamo in asteroid Vesta", *Science* **338** (2012), pp. 238–241.

[38] H.-C. Nataf, "Tidally synchronized solar dynamo: A rebuttal", *Solar Phys.* **297** (2022), article no. 107.

[39] E. Weisshaar, R. H. Cameron and M. Schüssler, "No evidence for synchronization of the solar cycle by a "clock"", *Astron. Astrophys.* **671** (2023), article no. A87.

[40] C.-C. Hung, *Apparent relations between solar activity and solar tides caused by the planets*, tech. rep., NASA, 2007. no. NASA/TM-2007-214817.

[41] N. Scafetta, "Does the Sun work as a nuclear fusion amplifier of planetary tidal forcing? A proposal for a physical mechanism based on the mass-luminosity relation", *J. Atmos. Sol.-Terr. Phys.* **81-82** (2012), pp. 27–40.

[42] I. R. G. Wilson, "The Venus-Earth-Jupiter spin-orbit coupling model", *Pattern Recogn. Phys.* **1** (2013), pp. 147–158.

[43] V. P. Okhlopkov, "The gravitational influence of Venus, the Earth, and Jupiter on the 11-year cycle of solar activity", *Mosc. Univ. Phys. Bull.* **71** (2016), pp. 440–446.

[44] F. Stefani, A. Giesecke, N. Weber and T. Weier, "Synchronized helicity oscillations: a link between planetary tides and the solar cycle?", *Solar Phys.* **291** (2016), pp. 2197–2212.

[45] F. Stefani, A. Giesecke and T. Weier, "A model of a tidally synchronized solar dynamo", *Solar Phys.* **294** (2019), article no. 60.

[46] F. Stefani, R. Stepanov and T. Weier, "Shaken and Stirred: When Bond Meets Suess–de Vries and Gnevyshev–Ohl", *Solar Phys.* **296** (2021), article no. 88.

[47] P. Charbonneau, "External forcing of the solar dynamo", *Front. Astron. Space Sci.* **9** (2022), article no. 853676.

[48] M. Klevs, L. Jouve, F. Stefani and T. Weier, "A synchronized two-dimensional $\alpha - \Omega$ model of the solar dynamo", *Solar Phys.* **298** (2023), article no. 90.

[49] G. Horstmann, G. Mamatsashvili, A. Giesecke, T. Zaqarashvili and F. Stefani, "Tidally forced planetary waves in the tachocline of solar-like stars", *Astrophys. J.* **944** (2023), article no. 48.

[50] F. Stefani, G. Horstmann, G. Mamatsashvili and T. Weier, "Rieger, Schwabe, Suess–de Vries: The sunny beats of resonance", *Solar Phys.* **299** (2024), article no. 51.

[51] J. H. Shirley, "Orbit-spin coupling and the circulation of the Martian atmosphere", *Planet. Space Sci.* **141** (201), pp. 1–16.

[52] J. H. Shirley, "Orbit-spin coupling, the solar dynamo, and the planetary theory of sunspots", 2023. *preprint*, arXiv:2309.13076.

[53] J. Vidal and D. Cébron, "Inviscid instabilities in rotating ellipsoids on eccentric Kepler orbits", *J. Fluid Mech.* **833** (2017), pp. 469–511.

[54] S. Horn and J. M. Aurnou, "Rotating convection with centrifugal buoyancy: Numerical predictions for laboratory experiments", *Phys. Rev. Fluids* **4** (2019), article no. 073501.

[55] T. Sloudsky, "De la rotation de la terre supposée fluide à son intérieur", *Bull. Soc. Imp. Natur. Mosc.* **2** (1895), pp. 285–318.

[56] H. Poincaré, "Sur la précession des corps déformables", *Bull. Astron.* **27** (1910), pp. 321–356.

[57] F. Busse, "Steady fluid flow in a precessing spheroidal shell", *J. Fluid Mech.* **33** (1968), pp. 739–751.

[58] R. Manasseh, "Breakdown regimes of inertia waves in a precessing cylinder", *J. Fluid Mech.* **243** (1992), pp. 261–296.

[59] J. J. Kobine, "Azimuthal flow associated with inertial wave resonance in a precessing cylinder", *J. Fluid Mech.* **319** (1996), pp. 387–406.

[60] Y. Lin, J. Noir and A. Jackson, "Experimental study of fluid flows in a precessing cylindrical annulus", *Phys. Fluids* **26** (2014), article no. 046604.

[61] W. Mouhali, T. Lehner, J. Léorat and R. Vitry, "Evidence of a cyclonic regime in a precessing cylindrical container", *Exp. Fluids* **53** (2012), pp. 1693–1700.

[62] S. Goto, A. Matsunaga, M. Fujiwara, et al., "Turbulence driven by precession in spherical and slightly elongated spheroidal cavities", *Phys. Fluids* **26** (2014), article no. 055107.

[63] J. Herault, T. Gundrum, A. Giesecke and F. Stefani, "Subcritical transition to turbulence of a precessing flow in a cylindrical vessel", *Phys. Fluids* **27** (2015), article no. 124102.

[64] K. Komoda and S. Goto, "Three-dimensional flow structures of turbulence in precessing spheroids", *Phys. Rev. Fluids* **4** (2019), article no. 014603.

[65] C. Nobili, P. Meunier, B. Favier and M. Le Bars, "Hysteresis and instabilities in a spheroid in precession near the resonance with the tilt-over mode", *J. Fluid Mech.* **909** (2021), article no. A17.

[66] J. Noir and D. Cébron, "Precession-driven flows in non-axisymmetric ellipsoids", *J. Fluid Mech.* **737** (2013), pp. 412–439.

[67] F. Burmann and J. Noir, "Experimental study of the flows in a non-axisymmetric ellipsoid under precession", *J. Fluid Mech.* **923** (2022), article no. A24.

[68] A. Tilgner, "Precession driven dynamos", *Phys. Fluids* **17** (2005), article no. 034104.

[69] C.-C. Wu and P. H. Roberts, "On a dynamo driven by topographic precession", *Geophys. Astrophys. Fluid Dyn.* **103** (2009), pp. 467–501.

[70] A. Krauze, "Numerical modeling of the magnetic field generation in a precessing cube with a conducting melt", *Magnetohydrodynamics* **46** (2010), pp. 271–280.

[71] C. Nore, J. Léorat, J.-L. Guermond and F. Luddens, "Nonlinear dynamo action in a precessing cylindrical container", *Phys. Rev. E* **93** (2011), article no. 043113.

[72] Y. Lin, P. Marti, J. Noir and A. Jackson, "Precession-driven dynamos in a full sphere and the role of large scale cyclonic vortices", *Phys. Fluids* **28** (2016), article no. 066601.

[73] O. Goepfert and A. Tilgner, "Dynamos in precessing cubes", *New J. Phys.* **18** (2016), article no. 103019.

[74] A. Giesecke, T. Vogt, T. Gundrum and F. Stefani, "Nonlinear large scale flow in a precessing cylinder and its ability to drive dynamo action", *Phys. Rev. Lett.* **120** (2018), article no. 024502.
[75] J. Vidal and D. Cébron, "Kinematic dynamos in triaxial ellipsoids", *Proc. R. Soc. Lond., Ser. A* **A477** (2021), article no. 20210252.
[76] R. F. Gans, "On hydromagnetic precession in a cylinder", *J. Fluid Mech.* **45** (1971), pp. 111–130.
[77] A. Tilgner, "On models of precession driven core flow", *Stud. Geophys. Geod.* **42** (1998), pp. 232–238.
[78] P. Meunier, C. Eloy, R. Lagrange and F. Nadal, "A rotating fluid cylinder subject to weak precession", *J. Fluid Mech.* **599** (2008), pp. 405–440.
[79] R. Lagrange, P. Meunier, F. Nadal and C. Eloy, "Precessional instability of a fluid cylinder", *J. Fluid Mech.* **666** (2011), pp. 104–145.
[80] D. Gao, P. Meunier, S. L. Dizès and C. Eloy, "Zonal flow in a resonant precessing cylinder", *J. Fluid Mech.* **923** (2021), article no. A29.
[81] J. J. Kobine, "Inertial wave dynamics in a rotating and precessing cylinder", *J. Fluid Mech.* **303** (1995), pp. 233–252.
[82] A. Giesecke, T. Albrecht, T. Gundrum, J. Herault and F. Stefani, "Triadic resonances in nonlinear simulations of a fluid flow in a precessing cylinder", *New J. Phys.* **17** (2015), article no. 113044.
[83] J. M. Lopez and F. Marquez, "Nonlinear and detuning effects of the nutation angle in precessionally forced rotating cylinder flow", *Phys. Rev. Fluids* **1** (2016), article no. 023602.
[84] T. Albrecht, H. M. Blackburn, J. M. Lopez, R. Manasseh and P. Meunier, "On triadic resonance as an instability mechanism in precessing cylinder flow", *J. Fluid Mech.* **841** (2018), article no. R3.
[85] J. Herault, A. Giesecke, T. Gundrum and F. Stefani, "Instability of precession driven Kelvin modes: Evidence of a detuning effect", *Phys. Rev. Fluids* **4** (2019), article no. 033901.
[86] R. Lagrange, C. Eloy, F. Nadal and P. Meunier, "Instability of a fluid inside a precessing cylinder", *Phys. Fluids* **20** (2008), article no. 081701.
[87] P. Meunier, "Geoinspired soft mixers", *J. Fluid Mech.* **903** (2020), article no. A15.
[88] H. Blackburn, D. Lee, T. Albrecht and J. Singh, "Semtex: A spectral element–fourier solver for the incompressible Navier–Stokes equations in cylindrical or cartesian coordinates", *Comput. Phys. Commun.* **245** (2019), article no. 106804.
[89] A. Giesecke, F. Stefani and G. Gerbeth, "Kinematic simulation of dynamo action by a hybrid boundary-element/finite-volume method", *Magnetohydrodynamics* **44** (2008), pp. 237–252.
[90] F. Ravelet, A. Chiffaudel, F. Daviaud and J. Léorat, "Toward an experimental von Kármán dynamo: Numerical studies for an optimized design", *Phys. Fluids* **17** (2005), article no. 117104.
[91] F. Stefani, M. Xu, G. Gerbeth, et al., "Ambivalent effects of added layers on steady kinematic dynamos in cylindrical geometry: application to the VKS experiment", *Eur. J. Mech. B Fluids* **25** (2006), pp. 894–908.
[92] A. Giesecke, F. Stefani and G. Gerbeth, "Influence of high-permeability discs in an axisymmetric model of the Cadarache dynamo experiment", *New J. Phys.* **14** (2012), article no. 053005.
[93] A. Giesecke, T. Vogt, T. Gundrum and F. Stefani, "Kinematic dynamo action of a precession-driven flow based on the results of water experiments and hydrodynamic simulations", *Geophys. Astrophys. Fluid Dyn.* **113** (2019), pp. 235–255.
[94] F. Pizzi, A. Giesecke, J. Šimkanin and F. Stefani, "Prograde and retrograde precession of a fluid-filled cylinder", *New J. Phys.* **23** (2021), article no. 123016.
[95] V. Kumar, F. Pizzi, A. Giesecke, et al., "The effect of nutation angle on the flow inside a precessing cylinder and its dynamo action", *Phys. Fluids* **35** (2023), article no. 014114.
[96] F. Pizzi, A. Giesecke, J. Šimkanin, V. Kumar, T. Gundrum and F. Stefani, "Numerical and theoretical framework for the DRESDYN precession dynamo experiments", *Magnetohydrodynamics* **58** (2022), pp. 445–453.
[97] M. M. Adams, D. R. Stone, D. S. Zimmerman and D. P. Lathrop, "Liquid sodium models of the Earth's core", *Prog. in Earth and Planet. Sci.* **2** (2015), article no. 29.
[98] D. B. Weisberg, E. Peterson, J. Milhone, et al., "Driving large magnetic Reynolds number flow in highly ionized, unmagnetized plasmas", *Phys. Plasmas* **24** (2017), article no. 056502.
[99] S. Rother and M. Beitelschmidt, "Strength assessment of a precession driven dynamo", *Tech. Mech.* **37** (2017), pp. 120–128.
[100] F. Stefani, T. Albrecht, G. Gerbeth, et al., "Towards a precession driven dynamo experiment", *Magnetohydrodynamics* **51** (2015), pp. 275–284.
[101] S. Rother and M. Beitelschmidt, "Input reduction for nonlinear thermal surface loads", *Arch. Appl. Mech.* **93** (2023), pp. 1863–1878.
[102] M. Wilbert, A. Giesecke and R. Grauer, "Numerical investigation of the flow inside a precession driven cylindrical cavity with additional baffles using an immersed boundary method", *Phys. Fluids* **34** (2022), article no. 96607.
[103] F. Burmann and J. Noir, "Effects of bottom topography on the spin-up in a cylinder", *Phys. Fluids* **30** (2018), article no. 106601.

[104] N. Saito, C. Liao and T. Tsuruda, "Ignition and extinguishment of sodium fires in air diluted by nitrogen", in *Proceedings, 5th AOSFST, Newcastle, Australia, 2001* (M. A. Delichatsios, B. Z. Dlugogorski and E. M. Kennedy, eds.), International Association for Fire Safety Science, 2001, pp. 285–294.

[105] K. Rahbarnia, B. P. Brown, M. M. Clark, et al., "Direct observation of the turbulent emf and transport of magnetic field in a liquid sodium experiment", *Astrophys. J.* **759** (2012), article no. 80.